

# Circuit Quantum Electrodynamics: Coherent Coupling of a Single Photon to a Cooper Pair Box

A. Wallraff, D. Schuster, A. Blais, L. Frunzio, R.-S. Huang,\* J. Majer, S. Kumar, S. M. Girvin, and R. J. Schoelkopf  
*Departments of Applied Physics and Physics, Yale University, New Haven, CT 06520*

(Dated: December 2, 2024, accepted for publication in *Nature (London)*)

Under appropriate conditions, superconducting electronic circuits behave quantum mechanically, with properties that can be designed and controlled at will. We have realized an experiment in which a superconducting two-level system, playing the role of an artificial atom, is strongly coupled to a single photon stored in an on-chip cavity. We show that the atom-photon coupling in this circuit can be made strong enough for coherent effects to dominate over dissipation, even in a solid state environment. This new regime of matter light interaction in a circuit can be exploited for quantum information processing and quantum communication. It may also lead to new approaches for single photon generation and detection.

The interaction of matter and light is one of the fundamental processes occurring in nature. One of its most elementary forms is realized when a single atom interacts with a single photon. Reaching this regime has been a major focus of research in atomic physics and quantum optics<sup>1</sup> for more than a decade and has created the field of cavity quantum electrodynamics<sup>2</sup> (CQED). In this article we show for the first time that this regime can be realized in a solid state system, where we have experimentally observed the coherent interaction of a superconducting two-level system with a single microwave photon. This new paradigm of *circuit quantum electrodynamics* may open many new possibilities for studying the strong interaction of light and matter.

In atomic cavity QED an isolated atom with electric dipole moment  $d$  interacts with the vacuum state electric field  $E_0$  of a cavity. The quantum nature of the electromagnetic field gives rise to coherent oscillations of a single excitation between the atom and the cavity at the vacuum Rabi frequency  $\nu_{\text{Rabi}} = 2dE_0/h$ , which can be observed experimentally when  $\nu_{\text{Rabi}}$  exceeds the rates of relaxation and decoherence of both the atom and the field. This effect has been observed both in the time domain using large dipole moment Rydberg atoms in 3D microwave cavities<sup>3</sup> and spectroscopically using alkali atoms in very small optical cavities with large vacuum fields<sup>4,5</sup>.

Our experimental implementation of cavity quantum electrodynamics in a circuit consists of a fully electrically controllable superconducting quantum two-level system, the Cooper pair box<sup>6</sup>, coupled to a single mode of the quantized radiation field in an on-chip cavity formed by a superconducting transmission line resonator. Coherent quantum effects have been recently observed in several superconducting circuits<sup>7,8,9,10,11,12</sup>, making these systems well suited for use as quantum bits (qubits) for quantum information processing<sup>13,14</sup>. Of these superconducting qubits, the Cooper pair box is especially well suited for cavity QED because of its large effective electric dipole moment  $d$ , which can be made more than  $10^4$  times larger than in an alkali atom in the ground state and still 10 times larger than in a typical Rydberg atom. In addition, the small size of the

quasi one-dimensional transmission line cavity used in our experiments generates a large vacuum electric field  $E_0$ . As suggested in our earlier theoretical study<sup>15</sup>, the simultaneous combination of large dipole moment and large field strength in our implementation is ideal for reaching the strong coupling limit of cavity QED in a circuit. Other solid state analogs of strong coupling cavity QED have been envisaged by many authors in superconducting<sup>16,17,18,19,20,21,22,23</sup>, semiconducting<sup>24,25</sup> and even micro-mechanical systems<sup>26,27</sup>. First steps towards realizing such a regime have been made for semiconductors<sup>24,28,29</sup>. Our experiments constitute the first experimental observation of strong coupling cavity QED with a *single* artificial atom and a *single* photon in a solid state system.

## I. THE CAVITY QED CIRCUIT

The on-chip cavity is realized as a distributed transmission line resonator patterned into a thin superconducting film deposited on the surface of a silicon chip. The quasi-one-dimensional coplanar waveguide resonator<sup>30</sup> consists of a narrow center conductor of length  $l$  and two nearby lateral ground planes, see Fig. 1a. Its full wave resonance occurs at a frequency of  $\nu_r = 6.04$  GHz. Close to its resonance frequency  $\omega_r = 2\pi\nu_r = 1/\sqrt{LC}$  the resonator can be modelled as a parallel combination of a capacitor  $C$  and an inductor  $L$  (a resistor  $R$  can be omitted since the internal losses are small). This simple resonant circuit behaves as a harmonic oscillator described by the Hamiltonian  $H_r = \hbar\omega_r(a^\dagger a + 1/2)$ , where  $a^\dagger$  ( $a$ ) is the creation (annihilation) operator for a single photon in the electromagnetic field and  $\langle a^\dagger a \rangle = \langle \hat{n} \rangle = n$  is the average photon number. Cooling such a resonator down to temperatures well below  $T^* = \hbar\omega_r/k_B \approx 300$  mK, the average photon number  $n$  can be made very small. At our operating temperatures of  $T < 100$  mK the thermal occupancy is  $n < 0.06$ , so the resonator is near its quantum ground state. The vacuum fluctuation energy stored in the resonator in the ground state gives rise to an effective rms voltage of  $V_{\text{rms}} = \sqrt{\hbar\omega_r/2C} \approx 1 \mu\text{V}$  on its center conduc-

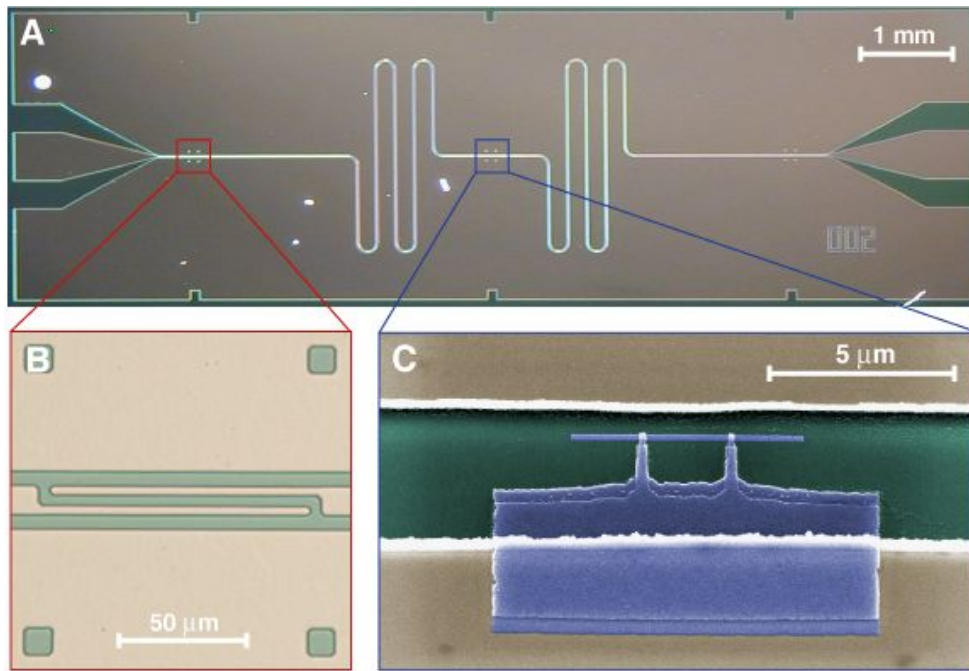


FIG. 1: Integrated circuit for cavity QED. **a** The superconducting niobium coplanar waveguide resonator is fabricated on an oxidized  $10 \times 3 \text{ mm}^2$  silicon chip using optical lithography. The width of the center conductor is  $w = 10 \mu\text{m}$  separated from the lateral ground planes extending to the edges of the chip by a gap of width  $d = 5 \mu\text{m}$  resulting in a wave impedance of the structure of  $Z = 50 \Omega$  being optimally matched to conventional microwave components. The length of the meandering resonator is  $l = 24 \text{ mm}$ . It is coupled by a capacitor at each end of the resonator (see **b**) to an input and output feed line, fanning out to the edge of the chip and keeping the impedance constant. **b** The capacitive coupling to the input and output lines and hence the coupled quality factor  $Q$  is controlled by adjusting the length and separation of the finger capacitors formed in the center conductor. **c** False color electron micrograph of a Cooper pair box (blue) fabricated onto the silicon substrate (green) into the gap between the center conductor (top) and the ground plane (bottom) of a resonator (beige) using electron beam lithography and double angle evaporation of aluminum. The Josephson tunnel junctions are formed at the overlap between the long thin island parallel to the center conductor and the fingers extending from the much larger reservoir coupled to the ground plane.

tor. The magnitude of the electric field between the center conductor and the ground plane in the vacuum state is then a remarkable  $E_{\text{rms}} \approx 0.2 \text{ V/m}$ , which is some 100 times larger than in atomic microwave cavity QED<sup>3</sup>. The large vacuum field strength resulting from the extremely small effective mode volume ( $\sim 10^{-6}$  cubic wavelengths) of the resonator is clearly advantageous for cavity QED not only in solid state but also in atomic systems<sup>31</sup>. In our experiments this vacuum field is coupled capacitively to a superconducting qubit. At the full wave resonance the electric field has antinodes at both ends and at the center of the resonator and its magnitude is maximal in the gap between the center conductor and the ground plane where we place our qubit.

The resonator is coupled via two coupling capacitors  $C_{\text{in/out}}$ , one at each end, see Fig. 1b, to the input and output transmission lines through which its microwave transmission can be probed, see Fig. 2a. The predominant source of dissipation is the loss of photons from the resonator through these input and output ports at a rate  $\kappa = \omega_r/Q$ , where  $Q$  is the (loaded) quality factor of the resonator. The internal (uncoupled) loss of the resonator

is negligible ( $Q_{\text{int}} \approx 10^6$ ). Thus, the average photon lifetime in the resonator  $T_r = 1/\kappa$  exceeds 100 ns even for moderate quality factors of  $Q \approx 10^4$ .

Our choice of artificial atom is a mesoscopic superconducting electrical circuit, the Cooper pair box<sup>6</sup> (CPB), the quantum properties of which have been clearly demonstrated<sup>7,16,32</sup>. The Cooper pair box consists of a several micron long and sub-micron wide superconducting island which is coupled via two sub-micron size Josephson tunnel junctions to a much larger superconducting reservoir. We have fabricated such a structure into the gap between the center conductor and the ground plane in the center section of the coplanar waveguide resonator, see Fig. 1c.

The Cooper Pair box is a tunable two-state system described by the Hamiltonian  $H_a = -1/2 (E_{\text{el}} \sigma_x + E_J \sigma_z)$ , where  $E_{\text{el}}$  is the electrostatic energy and  $E_J$  is the Josephson energy of the circuit. The electrostatic energy  $E_{\text{el}} = 4E_C (1 - n_g)$  is proportional to the charging energy  $E_C = e^2/2C_\Sigma$ , where  $C_\Sigma$  is the total capacitance of the island.  $E_{\text{el}}$  can be tuned by a gate charge  $n_g = V_g C_g^*/e$ , where  $V_g$  is the voltage applied to the input

port of the resonator and  $C_g^*$  the effective dc-capacitance between the input port of the resonator and the island of the Cooper pair box. The Josephson energy  $E_J = E_{J,\max} \cos(\pi\Phi_b)$  is proportional to  $E_{J,\max} = h\Delta/8e^2R_J$ , where  $\Delta$  is the superconducting gap and  $R_J$  is the tunnel junction resistance. Using an external coil,  $E_J$  can be tuned by applying a flux bias  $\Phi_b = \Phi/\Phi_0$  to the loop formed by the two tunnel junctions, the island and the reservoir. We denote the ground state of this system as  $|\downarrow\rangle$  and the excited state as  $|\uparrow\rangle$ , see Fig. 2d. The energy level separation between these two states is then given by  $E_a = \hbar\omega_a = \sqrt{E_{J,\max}^2 \cos^2(\pi\Phi_b) + 16E_C^2(1-n_g)^2}$ .

The Hamiltonian  $H_a$  of the Cooper pair box can be readily engineered by choosing the parameters  $E_{J,\max}$  and  $E_C$  during fabrication and by tuning the gate charge  $n_g$  and the flux bias  $\Phi_b$  in situ during experiment. The quantum state of the Cooper pair box can be manipulated using microwave pulses<sup>7,33</sup>. Coherence in the Cooper pair box is limited both by relaxation from the excited state  $|\uparrow\rangle$  into the ground state  $|\downarrow\rangle$  at a rate  $\gamma_1$  corresponding to a lifetime of  $T_1 = 1/\gamma_1$  and by fluctuations in the level separation giving rise to dephasing at a rate  $\gamma_\varphi$  corresponding to a dephasing time  $T_\varphi = 1/\gamma_\varphi$ . The total decoherence rate  $\gamma = \gamma_1/2 + \gamma_\varphi$  has contributions from the coupling to fluctuations in the electromagnetic environment<sup>32,34</sup> but is possibly dominated by non-radiative processes. Relevant sources of dephasing include coupling to low frequency fluctuations of charges in the substrate or tunnel junction barrier and coupling to flux motion in the superconducting films.

## II. THE QUBIT-CAVITY COUPLING

The coupling between the radiation field stored in the resonator and the Cooper pair box is realized through the coupling capacitance  $C_g$ . A voltage  $V_{\text{rms}}$  on the center conductor of the resonator changes the energy of an electron on the island of the Cooper pair box by an amount  $\hbar g = eV_{\text{rms}}C_g/C_\Sigma$ , where  $g$  is the coupling strength. The energy  $\hbar g$  is the dipole interaction energy  $dE_0$  between the qubit and the vacuum field in the resonator. We have shown<sup>15</sup> that the Hamiltonian describing this coupled system has the form  $H_{\text{JC}} = H_r + H_a + \hbar g(a^\dagger\sigma^- + a\sigma^+)$ , where  $\sigma^+$  ( $\sigma^-$ ) creates (annihilates) an excitation in the Cooper pair box. The Jaynes-Cummings Hamiltonian,  $H_{\text{JC}}$ , describing our coupled circuit is well known from cavity QED. It describes the coherent exchange of energy between a quantized electromagnetic field and a quantum two-level system at a rate  $g/2\pi$ , which is observable if  $g$  is much larger than the decoherence rates  $\gamma$  and  $\kappa$ . This situation is achieved in our experiments and is referred to as the strong coupling limit ( $g > [\gamma, \kappa]$ ) of cavity QED<sup>35</sup>. If such a system is prepared with the electromagnetic field in its ground state  $|0\rangle$ , the two-level system in its excited state  $|\uparrow\rangle$  and the two constituents are in resonance  $\omega_a = \omega_r$ , it oscillates between states  $|0, \uparrow\rangle$  and  $|1, \downarrow\rangle$  at

the vacuum Rabi frequency  $\nu_{\text{Rabi}} = g/\pi$ . In this situation the eigenstates of the coupled system are symmetric and antisymmetric superpositions of a single photon in a resonator and an excitation in the Cooper pair box  $|\pm\rangle = (|0, \uparrow\rangle \pm |1, \downarrow\rangle)/\sqrt{2}$  with energies  $E_\pm = \hbar(\omega_r \pm g)$ . Although the eigenstates  $|\pm\rangle$  are entangled, their entangled character is not addressed in our current CQED experiment. In our experiment, it is the energies  $E_\pm$  of the coherently coupled system which are probed spectroscopically.

In the non-resonant ('dispersive') case the qubit is detuned by an amount  $\Delta = \omega_a - \omega_r$  from the cavity resonance. The strong coupling between the field in the resonator and the Cooper pair box can be used to perform a quantum nondemolition (QND) measurement of the quantum state of the Cooper pair box. For  $|\Delta| \gg g$ , diagonalization of the coupled quantum system leads to the effective Hamiltonian<sup>15</sup>

$$H \approx \hbar \left( \omega_r + \frac{g^2}{\Delta} \sigma_z \right) a^\dagger a + \frac{1}{2} \hbar \left( \omega_a + \frac{g^2}{\Delta} \right) \sigma_z,$$

where the terms proportional to  $a^\dagger a$  determine the resonator properties and the terms proportional to  $\sigma_z$  determine the circuit properties. It is easy to see that the transition frequency of the resonator  $\omega_r \pm g^2/\Delta$  is conditioned by the qubit state  $\sigma_z = \pm 1$  and depends on the coupling strength  $g$  and the detuning  $\Delta$ . Thus by measuring the transition frequency of the resonator the qubit state can be determined. Similarly, the level separation in the qubit  $\Delta E_a = \hbar(\omega_a + 2a^\dagger a g^2/\Delta + g^2/\Delta)$  is conditioned by the number of photons in the resonator. The term  $2a^\dagger a g^2/\Delta$  linear in the photon number  $\hat{n}$  is known as the ac-Stark shift and the term  $g^2/\Delta$  as the Lamb shift as in atomic physics. All terms in this Hamiltonian, with the exception of the Lamb shift, are clearly identified in the results of our circuit QED experiments.

## III. THE MEASUREMENT TECHNIQUE

The properties of this strongly coupled circuit QED system are determined by probing the level separation of the resonator states spectroscopically<sup>15</sup>. The amplitude  $T$  and phase  $\phi$  of a microwave probe beam of power  $P_{\text{RF}}$  transmitted through the resonator are measured versus probe frequency  $\omega_{\text{RF}}$ . A simplified schematic of the basic microwave circuit is shown in Fig. 2a. In this setup the Cooper pair box acts as a circuit element that has an effective capacitance which is dependent on its  $\sigma_z$  eigenstate, the coupling strength  $g$ , and its detuning  $\Delta$ . It is connected through  $C_g$  in parallel with the resonator. This variable capacitance changes the resonance frequency of the resonator which can be probed by measuring its microwave transmission spectrum. The transmission  $T^2$  and phase  $\phi$  of the resonator for a far detuned qubit ( $g^2/\Delta\kappa \ll 1$ ), i.e. when the qubit is effectively decoupled from the resonator, are shown in Figs. 2b and c. In this case, the transmission is a Lorentzian line of

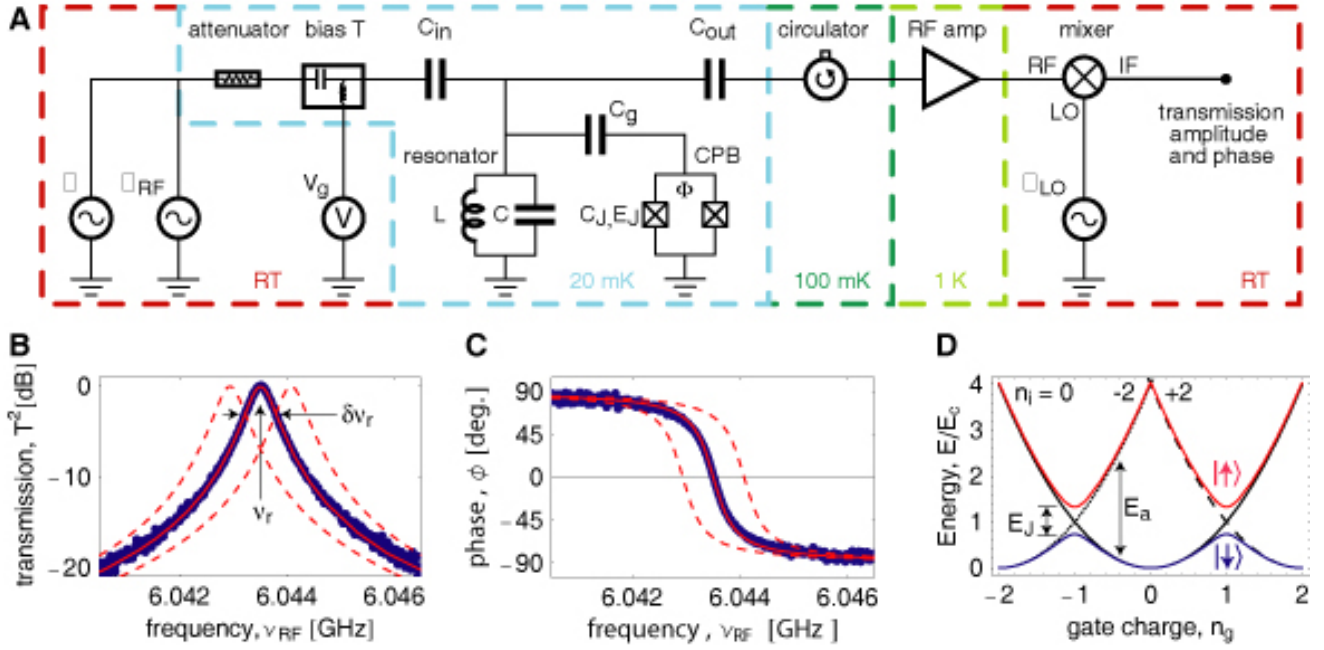


FIG. 2: Measurement scheme, resonator and Cooper pair box. **a** The resonator with effective inductance  $L$  and capacitance  $C$  coupled through the capacitor  $C_g$  to the Cooper pair box with junction capacitance  $C_J$  and Josephson energy  $E_J$  forms the circuit QED system which is coupled through  $C_{in/out}$  to the input/output ports. The value of  $E_J$  is controllable by the magnetic flux  $\Phi$ . The input microwaves at frequencies  $\omega$  and  $\omega_{RF}$  are added to the gate voltage  $V_g$  using a bias-tee. After the transmitted signal at  $\omega_{RF}$  is amplified using a cryogenic high electron mobility (HEMT) amplifier and mixed with the local oscillator at  $\omega_{LO}$ , its amplitude and phase are determined. The circulator and the attenuator prevent leakage of thermal radiation into the resonator. The temperature of individual components is indicated. **b** Measured transmission power spectrum of the resonator (blue dots), the full line width  $\delta\nu_r$  at half maximum and the center frequency  $\nu_r$  are indicated. The solid red line is fit to a Lorentzian with  $Q = \nu_r/\delta\nu_r \approx 10^4$ . **c** Measured transmission phase  $\phi$  (blue dots) with fit (red line). In panels b and c the dashed lines are theory curves shifted by  $\pm\delta\nu_r$  with respect to the data. **d** Energy level diagram of a Cooper pair box. The electrostatic energy  $(n_i - n_g)^2 e^2 / 2C_\Sigma$  is indicated for  $n_i = 0$  (solid black line),  $-2$  (dotted line) and  $+2$  (dashed line) excess electrons forming Cooper pairs on the island.  $C_\Sigma$  is the total capacitance of the island given by the sum of the capacitances  $C_J$  of the two tunnel junctions, the coupling capacitance  $C_g$  to the center conductor of the resonator and any stray capacitances. In such a system  $n_i$  is well determined if  $E_C/k_B$  is much larger than the bath temperature  $T$  and if the quantum fluctuations induced by the tunnelling of electrons through the junctions are small. In the absence of Josephson tunnelling the states with  $n_i$  and  $n_i + 2$  electrons on the island are degenerate at  $n_g = 1$ . The Josephson coupling mediated by the weak link formed by the tunnel junctions between the superconducting island and the reservoir lifts this degeneracy and opens up a gap proportional to the Josephson energy  $E_J$ . A ground state band  $|\downarrow\rangle$  and an excited state band  $|\uparrow\rangle$  are formed with a gate charge and flux bias dependent energy level separation of  $E_a$ .

width  $\delta\nu_r = \nu_r/Q$  at the resonance frequency  $\nu_r$  of the bare resonator. The transmission phase  $\phi$  displays a step of  $\pi$  at  $\nu_r$  with a width determined by  $Q$ . The expected transmission spectrum in both phase and amplitude for a frequency shift  $\pm g^2/\Delta$  of one resonator line width are shown by dashed lines in Fig. 2b and c. Such small shifts in the resonator frequency are sensitively measured in our experiments using probe beam powers  $P_{RF}$  which controllably populate the resonator with average photon numbers from  $n \approx 10^3$  down to the sub photon level  $n \ll 1$ . It is worth noting that in this architecture both the resonator and the qubit can be controlled and measured using capacitive and inductive coupling only, i.e. without attaching any dc-connections to either system.

#### IV. THE DISPERSIVE REGIME

In the dispersive regime, the qubit is detuned from the resonator by an amount  $\Delta$  and thus induces a shift  $g^2/\Delta$  in the resonance frequency which we measure as a phase shift  $\tan^{-1}(2g^2/\kappa\Delta)$  of the transmitted microwave at a fixed probe frequency  $\omega_{RF}$ . The detuning  $\Delta$  is controlled *in situ* by adjusting the gate charge  $n_g$  and the flux bias  $\Phi_b$  of the qubit. For a Cooper pair box with Josephson energy  $E_{J,max}/h > \nu_r$  two different cases can be identified. In the first case, for bias fluxes such that  $E_J(\Phi_b)/h > \nu_r$ , the qubit does not come into resonance with the resonator for any value of gate charge  $n_g$ , see Fig. 3a. As a result, the measured phase shift  $\phi$  is maximum for the smallest detuning  $\Delta$  at  $n_g = 1$  and gets smaller as the detuning  $\Delta$  increases, see Fig. 3b. More-

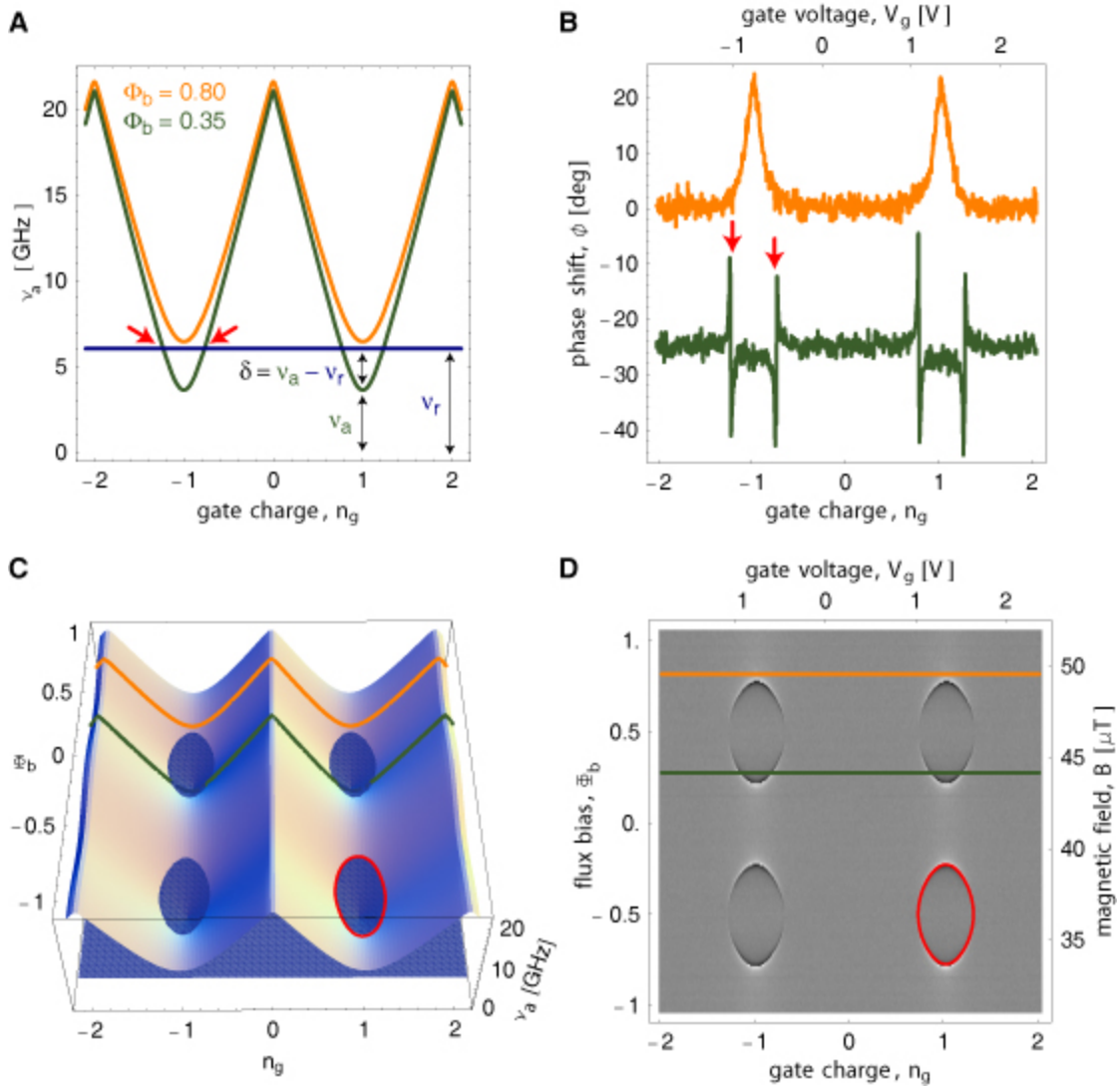


FIG. 3: Strong coupling circuit QED in the dispersive regime. **a** Calculated level separation  $\nu_a = \omega_a/2\pi = E_a/h$  between ground  $|\downarrow\rangle$  and excited state  $|\uparrow\rangle$  of qubit for two values of flux bias  $\Phi_b = 0.8$  (orange line) and  $\Phi_b = 0.35$  (green line). The resonator frequency  $\nu_r = \omega_r/2\pi$  is shown by a blue line. Resonance occurs at  $\nu_a = \nu_r$  symmetrically around degeneracy  $n_g = 1$ , see red arrows. The detuning  $\Delta/2\pi = \delta = \nu_a - \nu_r$  is indicated. **b** Measured phase shift  $\phi$  of the transmitted microwave for values of  $\Phi_b$  in a. Green curve is offset by  $-25$  deg for visibility. **c** Calculated qubit level separation  $\nu_a$  versus bias parameters  $n_g$  and  $\Phi_b$ . The resonator frequency  $\nu_r$  is indicated by the blue plane. At the intersection, also indicated by the red curve in the lower right hand quadrant, resonance between the qubit and the resonator occurs ( $\delta = 0$ ). For qubit states below the resonator plane the detuning is  $\delta < 0$ , above  $\delta > 0$ . **d** Density plot of measured phase shift  $\phi$  versus  $n_g$  and  $\Phi_b$ . Light colors indicate positive  $\phi$  ( $\delta > 0$ ), dark colors negative  $\phi$  ( $\delta < 0$ ). The red line is a fit of the data to the resonance condition  $\nu_a = \nu_r$ . In c and d, the line cuts presented in a and b are indicated by the orange and the green line, respectively. The microwave probe power  $P_{RF}$  used to acquire the data is adjusted such that the maximum intra resonator photon number  $n$  at  $\nu_r$  is about 10 for  $g^2/\Delta\kappa \ll 1$ . The calibration of the photon number has been performed in situ by measuring the ac-Stark shift of the qubit levels<sup>37</sup>.

over,  $\phi$  is periodic in  $n_g$  with a period of  $2e$ , as expected. In the second case, for values of  $\Phi_b$  resulting in  $E_J/h < \nu_r$ , the qubit goes through resonance with the resonator at two values of  $n_g$ . Thus, the phase shift  $\phi$  is largest as the qubit approaches resonance ( $\Delta \rightarrow 0$ ) at the points indicated by red arrows, see Fig. 3b. As the qubit goes through resonance, the phase shift  $\phi$  changes sign

as  $\Delta$  changes sign. This behavior is in perfect agreement with our predictions based on the analysis of the circuit QED Hamiltonian in the dispersive regime.

In Fig. 3c the qubit level separation  $\nu_a = E_a/h$  is plotted versus the bias parameters  $n_g$  and  $\Phi_b$ . The qubit is in resonance with the resonator ( $\nu_a = \nu_r$ ) at the set of parameters  $[n_g, \Phi_b]$  also indicated by the red curve in

one quadrant of the plot. The measured phase shift  $\phi$  is plotted versus both  $n_g$  and  $\Phi_b$  in Fig. 3d. We observe the expected periodicity in flux bias  $\Phi_b$  with one flux quantum  $\Phi_0$ . The set of parameters  $[n_g, \Phi_b]$  for which the resonance condition is met is marked by a sudden sign change in  $\phi$ . From this set, the Josephson energy  $E_{J,\max}$  and the charging energy  $E_C$  of the qubit can be determined in a fit to the resonance condition. Using the measured resonance frequency  $\nu_r = 6.044$  GHz, we extract the qubit parameters  $E_{J,\max} = 8.0 (\pm 0.1)$  GHz and  $E_C = 5.2 (\pm 0.1)$  GHz.

This set of data clearly demonstrates that the properties of the qubit in this strongly coupled system can be determined in a transmission measurement of the resonator and that full in situ control over the qubit parameters is achieved. We note that in the dispersive regime this new read-out scheme for the Cooper pair box is most sensitive at charge degeneracy ( $n_g = 1$ ), where the qubit is to first order decoupled from  $1/f$  fluctuations in its charge environment, which minimizes dephasing. This property is advantageous for quantum control of the qubit at  $n_g = 1$ , a point where traditional electrometry, using an SET for example<sup>32</sup>, is unable to distinguish the qubit states. Moreover, we note that this dispersive measurement scheme performs a quantum non-demolition read-out of the qubit state<sup>15</sup> which is the complement of the atomic microwave cQED measurement in which the state of the photon field is inferred non-destructively from the phase shift in the state of atoms sent through the cavity<sup>3,36</sup>.

## V. THE RESONANT REGIME

Making use of the full control over the qubit Hamiltonian, we tune the flux bias  $\Phi_b$  such that the qubit is at  $n_g = 1$  and in resonance with the resonator. Initially, the resonator and the qubit are cooled into their combined ground state  $|0, \downarrow\rangle$ , see inset in Fig. 4b. Due to the coupling, the first excited states become a doublet. We probe the energy splitting of this doublet spectroscopically using a microwave probe beam which populates the resonator with much less than one photon on average. The intra resonator photon number is calibrated measuring the ac-Stark shift of the qubit level separation in the dispersive case when probing the resonator at its maximum transmission<sup>37</sup>. The resonator transmission  $T^2$  is first measured for large detuning  $\Delta$  with a probe beam populating the resonator with a maximum of  $n \approx 1$  at resonance, see Fig. 4a. From the Lorentzian line the photon decay rate of the resonator is determined as  $\kappa/2\pi = 0.8$  MHz. The probe beam power is subsequently reduced by 5 dB and the transmission spectrum  $T^2$  is measured in resonance ( $\Delta = 0$ ), see Fig. 4b. We clearly observe two well resolved spectral lines separated by the vacuum Rabi frequency  $\nu_{\text{Rabi}} \approx 11.6$  MHz. The individual lines have a width determined by the average of the photon decay rate  $\kappa$  and the qubit decay rate  $\gamma$ .

The data is in excellent agreement with the transmission spectrum numerically calculated from the Jaynes-Cummings Hamiltonian characterizing the qubit decay and dephasing by the single parameter  $\gamma/2\pi = 0.7$  MHz.

In fact, the transmission spectrum shown in Fig. 4b is highly sensitive to the thermal photon number in the cavity. Due to the anharmonicity of the coupled atom-cavity system in the resonant case, an increased thermal photon number would reduce transmission and give rise to additional peaks in the spectrum due to transitions between higher excited doublets<sup>38</sup>. The transmission spectrum calculated for a thermal photon number of  $n = 0.5$ , see light blue curve in Fig. 4b, is clearly incompatible with our experimental data. The measured transmission spectrum, however, is consistent with the expected thermal photon number of  $n \lesssim 0.06$  ( $T < 100$  mK), see red curve in Fig. 4b, indicating that the coupled system has in fact cooled to near its ground state.

Similarly, multiphoton transitions between the ground state and higher excited doublets can occur at higher probe beam powers. Such transitions also probe the non-linearity of the cavity QED system. In our experiment these additional transitions are not resolved individually, but they do lead to a broadening of vacuum Rabi peaks with power. Eventually, at high drive powers the transmission spectrum becomes single peaked again as transitions between states high up in the dressed states ladder are driven.

We also observe the anti-crossing between the single photon resonator state and the first excited qubit state as the qubit is brought into resonance with the resonator at  $n_g = 1$  when tuning the gate charge and weakly probing the transmission spectrum, see Fig. 4c. For small deviations from  $n_g = 1$  the vacuum Rabi peaks evolve from a state with equal weight in the photon and qubit, as shown in Fig. 4b, to predominantly photon states for  $n_g \gg 1$  or  $n_g \ll 1$ . Throughout the full range of gate charge the observed peak positions agree well with calculations considering the qubit with level separation  $\nu_a$ , a single photon in the resonator with frequency  $\nu_r$  and a coupling strength of  $g/2\pi$ , see solid lines in Fig. 4c.

We have performed the same measurement for a different value of flux bias  $\Phi_b$  such that  $E_a/h < \nu_r$  at  $n_g = 1$ . The corresponding plot of the transmission amplitude shows two anti-crossings as the qubit is brought from large positive detuning  $\Delta$  through resonance and large negative detuning once again through resonance to positive detuning, see Fig. 4d. Again, the peak positions are in agreement with the theoretical prediction.

## VI. DISCUSSION

We have for the first time observed strong coupling cavity quantum electrodynamics at the level of a single qubit and a single photon in an all solid state system. We have demonstrated that the characteristic parameters of our novel circuit QED architecture can be chosen



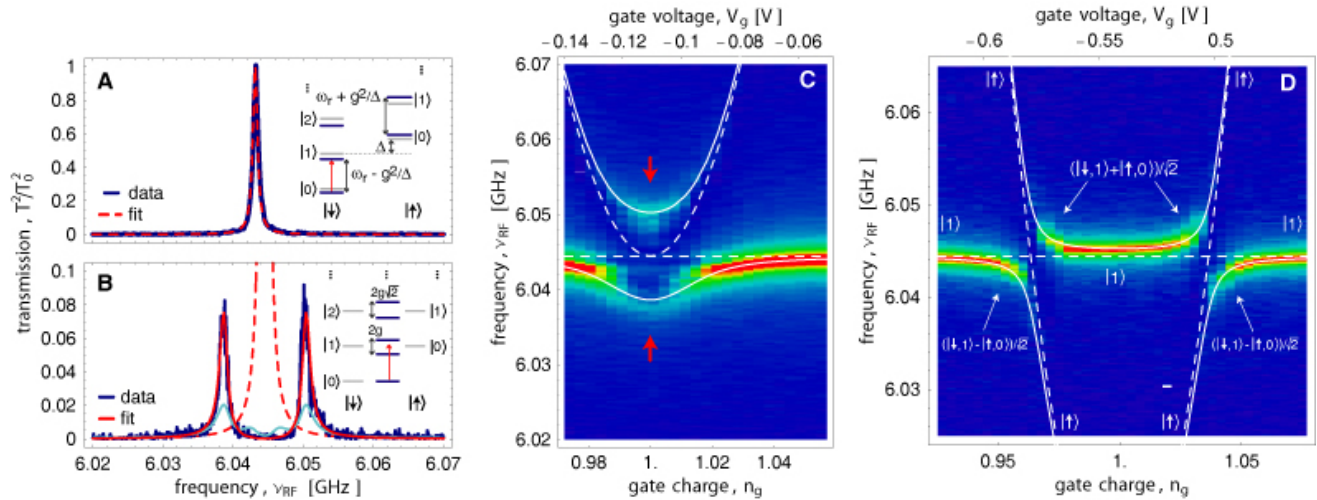


FIG. 4: Vacuum Rabi mode splitting. **a** Measured transmission  $T^2$  (blue line) versus microwave probe frequency  $\nu_{\text{RF}}$  for large detuning ( $g^2/\Delta\kappa \ll 1$ ) and fit to Lorentzian (dashed red line). The peak transmission amplitude is normalized to unity. The inset shows the dispersive dressed states level diagram. **b** Measured transmission spectrum for the resonant case  $\Delta = 0$  at  $n_g = 1$  (blue line) showing the Vacuum Rabi mode splitting compared to numerically calculated transmission spectra (red and light blue lines) for thermal photon numbers of  $n = 0.06$  and  $0.5$ , respectively. The dashed line is the calculated transmission for  $g = 0$  and  $\kappa/2\pi = 0.8$  MHz. The inset shows the resonant dressed states level diagram. **c** Resonator transmission amplitude  $T$  plotted versus probe frequency  $\nu_{\text{RF}}$  and gate charge  $n_g$  for  $\Delta = 0$  at  $n_g = 1$ . Dashed lines are uncoupled qubit level separation  $\nu_a$  and resonator resonance frequency  $\nu_r$ . Solid lines are level separations found from exact diagonalization of  $H_{\text{JC}}$ . Spectrum shown in **b** corresponds to line cut along red arrows. **d** As in **c**, but for  $E_J/h < \nu_r$ . The dominant character of the corresponding eigenstates is indicated.

at will during fabrication and can be fully controlled in situ during experiment. This system will open new possibilities to perform quantum optics experiments in solids. It also provides a novel architecture for quantum control and quantum measurement of electrical circuits and will find application in superconducting quantum computation, for example as a single-shot QND read-out of qubits and for coupling of qubits over centimeter distances using the resonator as a quantum bus. This architecture may readily be used to control, couple and read-out two qubits and can be scaled up to more complex circuits<sup>15</sup>. Non-radiative contributions to decoherence in solid state qubits can be investigated in this system by using the resonator to decouple the qubit from fluctuations in its electromagnetic environment. Finally, our circuit QED setup may potentially be used for generation and detection of single microwave photons in devices that could be applied in quantum communication.

## Acknowledgments

We thank John Teufel, Ben Turek and Julie Wyatt for their contributions to the project and are grateful to Peter Day, David DeMille, Michel Devoret, Sandy Weinreb and Jonas Zmuidzinas for numerous conversations. This work was supported in part by the National Security Agency (NSA) and Advanced Research and Development Activity (ARDA) under Army Research Office (ARO) contract number DAAD19-02-1-0045, the NSF ITR program under grant number DMR-0325580, the NSF under grant number DMR-0342157, the David and Lucile Packard Foundation, the W. M. Keck Foundation, and the Natural Science and Engineering Research Council of Canada (NSERC).

\* Department of Physics, Indiana University, Bloomington, IN 47405

<sup>1</sup> Walls, D. & Milburn, G. *Quantum optics*. Springer-Verlag, Berlin, (1994).

<sup>2</sup> Mabuchi, H. & Doherty, A. Cavity quantum electrodynamics: Coherence in context. *Science* **298**, 1372 (2002).

<sup>3</sup> Raimond, J., Brune, M., & Haroche, S. Manipulating quantum entanglement with atoms and photons in a cav-

ity. *Rev. Mod. Phys.* **73**, 565 (2001).

<sup>4</sup> Thompson, R. J., Rempe, G., & Kimble, H. J. Observation of normal-mode splitting for an atom in an optical cavity. *Phys. Rev. Lett.* **68**, 1132 (1992).

<sup>5</sup> Hood, C. J., Lynn, T. W., Doherty, A. C., Parkins, A. S., & Kimble, H. J. The atom-cavity microscope: Single atoms bound in orbit by single photons. *Science* **287**, 1447 (2000).

<sup>6</sup> Bouchiat, V., Vion, D., Joyez, P., Esteve, D., & Devoret,

- M. H. Quantum coherence with a single Cooper pair. *Physica Scripta* **T76**, 165 (1998).
- <sup>7</sup> Nakamura, Y., Pashkin, Y. A., & Tsai, J. S. Coherent control of macroscopic quantum states in a single-cooper-pair box. *Nature* **398**, 786–788 (1999).
  - <sup>8</sup> Vion, D., Aassime, A., Cottet, A., Joyez, P., Pothier, H., Urbina, C., Esteve, D., & Devoret, M. H. Manipulating the quantum state of an electrical circuit. *Science* **296**, 886 (2002).
  - <sup>9</sup> Martinis, J. M., Nam, S., Aumentado, J., & Urbina, C. Rabi oscillations in a large Josephson-junction qubit. *Phys. Rev. Lett.* **89**, 117901 (2002).
  - <sup>10</sup> Yu, Y., Han, S., Chu, X., Chu, S.-I., & Wang, Y. Coherent temporal oscillations of macroscopic quantum states in a Josephson junction. *Science* **296**, 889 (2002).
  - <sup>11</sup> Chiorescu, I., Nakamura, Y., Harmans, C. J. P. M., & Mooij, J. E. Coherent quantum dynamics of a superconducting flux qubit. *Science* **299**, 1869–1871 (2003).
  - <sup>12</sup> Yamamoto, T., Pashkin, Y. A., Astafiev, O., Nakamura, Y., & Tsai, J. S. Demonstration of conditional gate operation using superconducting charge qubits. *Nature* **425**, 941–944 (2003).
  - <sup>13</sup> Bennett, C. H. & DiVincenzo, D. P. Quantum information and computation. *Nature* **404**, 247–255 (2000).
  - <sup>14</sup> Nielsen, M. A. & Chuang, I. L. *Quantum computation and quantum information*. Cambridge University Press, (2000).
  - <sup>15</sup> Blais, A., Huang, R.-S., Wallraff, A., Girvin, S., & Schoelkopf, R. Cavity quantum electrodynamics for superconducting electrical circuits: an architecture for quantum computation. *Phys. Rev. A* **69**, – (2004). (in press).
  - <sup>16</sup> Makhlin, Y., Schön, G., & Shnirman, A. Quantum-state engineering with Josephson-junction devices. *Rev. Mod. Phys.* **73**, 357 (2001).
  - <sup>17</sup> Buisson, O. & Hekking, F. Entangled states in a Josephson charge qubit coupled to a superconducting resonator. In *Macroscopic Quantum Coherence and Quantum Computing*, Averin, D. V., Ruggiero, B., & Silvestrini, P., editors. Kluwer, New York, (2001).
  - <sup>18</sup> Marquardt, F. & Bruder, C. Superposition of two mesoscopically distinct quantum states: Coupling a Cooper-pair box to a large superconducting island. *Phys. Rev. B* **63**, 054514 (2001).
  - <sup>19</sup> Al-Saidi, W. A. & Stroud, D. Eigenstates of a small Josephson junction coupled to a resonant cavity. *Phys. Rev. B* **65**, 014512 (2001).
  - <sup>20</sup> Plastina, F. & Falci, G. Communicating Josephson qubits. *Phys. Rev. B* **67**, 224514 (2003).
  - <sup>21</sup> Blais, A., Maassen van den Brink, A., & Zagoskin, A. Tunable coupling of superconducting qubits. *Phys. Rev. Lett.* **90**, 127901 (2003).
  - <sup>22</sup> Yang, C.-P., Chu, S.-I., & Han, S. Possible realization of entanglement, logical gates, and quantum-information transfer with superconducting-quantum-interference-device qubits in cavity QED. *Phys. Rev. A* **67**, 042311 (2003).
  - <sup>23</sup> You, J. Q. & Nori, F. Quantum information processing with superconducting qubits in a microwave field. *Phys. Rev. B* **68**, 064509 (2003).
  - <sup>24</sup> Kiraz, A., Michler, P., Becher, C., Gayral, B., Imamoglu, A., Zhang, L. D., Hu, E., Schoenfeld, W. V., & Petroff, P. M. Cavity-quantum electrodynamics using a single InAs quantum dot in a microdisk structure. *Appl. Phys. Lett.* **78**, 3932–3934 (2001).
  - <sup>25</sup> Childress, L., Sørensen, A. S., & Lukin, M. D. Mesoscopic cavity quantum electrodynamics with quantum dots. *Phys. Rev. A* **69**, 042302 (2004).
  - <sup>26</sup> Armour, A., Blencowe, M., & Schwab, K. C. Entanglement and decoherence of a micromechanical resonator via coupling to a Cooper-pair box. *Phys. Rev. Lett.* **88**, 148301 (2002).
  - <sup>27</sup> Irish, E. K. & Schwab, K. Quantum measurement of a coupled nanomechanical resonator – Cooper-pair box system. *Phys. Rev. B* **68**, 155311 (2003).
  - <sup>28</sup> C. Weisbuch, M. Nishioka, A. I. & Arakawa, Y. Observation of the coupled exciton-photon mode splitting in a semiconductor quantum microcavity. *Phys. Rev. Lett.* **69**, 3314–3317 (1992).
  - <sup>29</sup> Vuckovic, J., Fattal, D., Santori, C., Solomon, G. S., & Yamamoto, Y. Enhanced single-photon emission from a quantum dot in a micropost microcavity. *Appl. Phys. Lett.* **82**, 3596 (2003).
  - <sup>30</sup> Day, P. K., LeDuc, H. G., Mazin, B. A., Vayonakis, A., & Zmuidzinas, J. A broadband superconducting detector suitable for use in large arrays. *Nature (London)* **425**, 817 (2003).
  - <sup>31</sup> Sørensen, A. S., van der Wal, C. H., Childress, L., & Lukin, M. D. Capacitive coupling of atomic systems to mesoscopic conductors. *Phys. Rev. Lett.* **92**, 063601 (2004).
  - <sup>32</sup> Lehnert, K., Bladh, K., Spietz, L., Gunnarsson, D., Schuster, D., Delsing, P., & Schoelkopf, R. Measurement of the excited-state lifetime of a microelectronic circuit. *Phys. Rev. Lett.* **90**, 027002 (2003).
  - <sup>33</sup> Nakamura, Y., Pashkin, Y. A., Yamamoto, T., & Tsai, J. S. Charge echo in a Cooper-pair box. *Phys. Rev. Lett.* **88**, 047901 (2002).
  - <sup>34</sup> Schoelkopf, R. J., Clerk, A. A., Girvin, S. M., Lehnert, K. W., & Devoret, M. H. *Quantum Noise*, chapter Qubits as Spectrometers of Quantum Noise. Kluwer Academic, Dordrecht (2003). cond-mat/0210247.
  - <sup>35</sup> Haroche, S. *Fundamental Systems in Quantum Optics*, chapter Cavity quantum electrodynamics, 767. Elsevier (1992).
  - <sup>36</sup> Noguees, G., Rauschenbeutel, A., Osnaghi, S., Brune, M., Raimond, J. M., & Haroche, S. Seeing a single photon without destroying it. *Nature (London)* **400**, 239–242 (1999).
  - <sup>37</sup> Schuster, D., Wallraff, A., & Schoelkopf, R. Measurement of the ac-Stark shift in a Cooper pair box. (unpublished) (2004).
  - <sup>38</sup> Rau, I., Johansson, G., & Shnirman, A. Cavity QED in superconducting circuits: susceptibility at elevated temperatures. cond-mat/0403257 (2004).